Research Article

Lawal Abubakar, Nor Azah Yusof*, Abdul Halim Abdullah, Mohd Hanif Wahid, Siti Fatimah Abd Rahman, Faruq Mohammad*, Hamad A. Al-Lohedan, and Ahmed A. Soleiman

Nanoporous carbon@$CoFe_2O_4$ nanocomposite as a green absorbent for the adsorptive removal of Hg(II) from aqueous solutions

https://doi.org/10.1515/gps-2023-0169
received September 14, 2023; accepted December 4, 2023

Abstract: To address the harmful pollutants found in heavy metals and agricultural waste, researchers have worked on creating various materials that can capture these pollutants. They have experimented with altering the shape, size, structure, surface properties, and bioactive components of these materials. This study aims to improve the effectiveness of materials used for adsorption, focusing on the combination of cobalt spinal ferrite ($CoFe_2O_4$) and nanoporous carbon (NC) obtained from discarded palm kernel shells with the aim of Hg(II) removal. The composite formed by the hydrothermal method was characterized thoroughly with morphological, structural, functional, pore sizes, thermal analysis, and magnetization analysis. Adsorption experiments were conducted under optimal conditions with a mass of 0.3 g, a concentration of 30 mg·L^{-1} of Hg(II), and a pH of 3. The aim was to adsorb Hg(II) ions from aqueous solutions. The analysis of kinetic studies using the Freundlich model revealed that it provided the most accurate fit for the adsorption isotherm. This model indicated a maximum Hg(II) adsorption efficiency of 232.56 mg·g^{-1}. Additionally, the thermodynamic measurements indicate that the adsorption is a spontaneous, favorable, and endothermic process. Likewise, we assessed how well the NC@$CoFe_2O_4$ nanocomposite could absorb Hg(II) ions in actual condensate samples from the oil and gas industry. The results demonstrated a 93% recovery rate for Hg(II) ions in wastewater. According to the findings, the NC@$CoFe_2O_4$ nanocomposite synthesized appears to be a strong contender for wastewater treatment and, at the same time, the prepared nanocomposite's effectiveness, affordability, and non-toxic nature support the potential applications.

Keywords: nanoporous carbon, $CoFe_2O_3$, magnetite nanoparticles, Hg(II) adsorption, thermodynamics, wastewater treatment

*** Corresponding author: Nor Azah Yusof,** Chemistry Department, Faculty of Science, Universiti Putra Malaysia, 43400 Serdang, Selangor, Malaysia; Institute of Nanoscience and Nanotechnology, Universiti Putra Malaysia, 43400 Serdang, Selangor, Malaysia, e-mail: azahy@upm.edu.my
*** Corresponding author: Faruq Mohammad,** Department of Chemistry, College of Science, King Saud University, Riyadh 11451, Saudi Arabia, e-mail: fmohammad@ksu.edu.sa, tel: +966 (0)11 467 5998
Lawal Abubakar: Chemistry Department, Faculty of Science, Universiti Putra Malaysia, 43400 Serdang, Selangor, Malaysia; Department of Chemistry, Shehu Shagari College of Education Sokoto, Sokoto, Nigeria
Abdul Halim Abdullah: Chemistry Department, Faculty of Science, Universiti Putra Malaysia, 43400 Serdang, Selangor, Malaysia; Institute of Nanoscience and Nanotechnology, Universiti Putra Malaysia, 43400 Serdang, Selangor, Malaysia
Mohd Hanif Wahid: Chemistry Department, Faculty of Science, Universiti Putra Malaysia, 43400 Serdang, Selangor, Malaysia
Siti Fatimah Abd Rahman: School of Electrical and Electronic Engineering, Engineering Campus, Universiti Sains Malaysia, 14300 Nibong Tebal, Pulau Pinang, Malaysia
Hamad A. Al-Lohedan: Department of Chemistry, College of Science, King Saud University, Riyadh 11451, Saudi Arabia
Ahmed A. Soleiman: College of Sciences and Engineering, Southern University, Baton Rouge, Louisiana 70813, USA

1 Introduction

The recent increase in industrialization has rapidly polluted the soil, water, and environment and therefore the United Nations (UN) sustainable development has set the goal of clean water and sanitation by 2030. This includes cleanliness and sanitation, wastewater treatment, water quality, water scarcity, unified water resources administration, and preserving and reinstating aquatic ecosystems [1]. Rapid urbanization and industrialization, especially in developing nations, pose a significant threat to the environment and human health due to heavy metal pollution. This is particularly concerning as polluted water bodies, which are a primary source of drinking water for many people, are heavily affected [2–4]. Metals like mercury, lead, zinc, arsenic, nickel, manganese, copper, cadmium, and chromium can cause cancer and are harmful

Open Access. © 2023 the author(s), published by De Gruyter. This work is licensed under the Creative Commons Attribution 4.0 International License.

substances [5,6]. They are emitted into the environment, particularly bodies of water, by various substances, including dyes, fertilizers, pesticides, and industrial products, contributing to water pollution, originating from both natural and human-made sources.

Mercury, specifically in its ionized form (Hg), is now recognized as a significant environmental threat to public health due to its extreme toxicity, both in immediate and prolonged exposure. Its ability to move through ecosystems poses a serious risk to the central nervous system, kidneys, lungs, and reproductive system. Thus, its debris could be found in the human body due to gastrointestinal absorption, skin contact, or pulmonary inhalation [7–9]. Hg(II) exposure can occur from natural and artificial sources and is released into bodies of water when no additional treatment is subjected to the polluted water [10,11]. However, combating pollution at its source and treating wastewater protects the public health environment, reduces the cost of pollution, and improves the water resource availability, in addition to recovering vital nutrients and water resources, as there is a need for modern techniques to overcome the risk of untreated wastewater containing Hg(II) [12]. Due to fast urban growth and increased industrial activity, the environment faces a serious problem from harmful substances like metals that are heavy and colored dyes. This is a major worry in poorer nations, where dirty water sources play a big role in providing drinking water to the population. For example, Nodehi and colleagues developed F_3O_4@NiO core–shell magnetic nanoparticles (NPs) to effectively eliminate alizarin red S dye from polluted wastewater [13], Congo red [14], anionic methyl orange [15], and cationic dyes [16]. However, $NiFe_2O_4$ and $NiFe_2O_4$/HNTs/GQD magnetic NPs were found to be effective for removing Cd(II) from water as a unique adsorbent [17,18].

To date, different kinds of materials have been applied as adsorbents, including polymers, nanocomposites, activated carbons, clays, graphene materials, and metal oxides like Al_2O_3, TiO_2, and SiO_2 [19]. Recently, magnetite NPs have sparked a lot of interest due to their unique physico-chemical properties, particularly strong magnetic quality, unique electrical characteristics, a spacious surface, and are very effective at absorbing substances. Due to their magnetic properties, magnetite NPs can be effortlessly extracted from water using a magnet. Additionally, the surface can be readily modified with different composite materials [20–22]. The magnetite NP materials are especially motivating for use in separating and removing mercury(II) due to their inspiring properties [23,24]. As shown in Table 1, many researchers used different magnetite NPs for Hg(II) removal and selectivity.

Cobalt spinel ferrites, also known as $CoFe_2O_4$, have gained significant attention from researchers due to their remarkable properties, including strong directionality in magnetism, high resistance to demagnetization, decent magnetic strength, and reliable stability under elevated temperatures. These attributes make them useful in a wide range of technological applications, including sensors, data storage devices, magnetic cards, solar panels, drug delivery systems, medical equipment, catalytic processes, and biotechnology [42–44]. Changing the coating

Table 1: Magnetite NPs for Hg(II) adsorption/removal

Magnetite NPs	Adsorption/removal	Temperature (°C)	Reference
γ-Fe_2O_3	140 mg·g^{-1}	30	[25]
Polyrhodanine-coated γ-Fe_2O_3	179 mg·g^{-1}	30	[25]
Fe_3O_4@SiO_2	98%		[26]
MPTS-CNTs/Fe_3O_4	65.52 mg·g^{-1}	25	[27]
Fe_2O_3–Al_2O_3	63.69 mg·g^{-1}		[28]
Fe_3O_4–GS	23.03 mg·g^{-1}		[29]
Water-soluble Fe_3O_4	99%	25	[30]
Fe_3O_4@C	83.1 mg·g^{-1}		[31]
EDTA–Fe_3O_4	203 mg·g^{-1}	25	[32]
Fe_3O_4@SiO_2-SH	132 mg·g^{-1}	25	[33]
NanoFe_3O_4@Nano-SiO_2	100 μmol·g^{-1}		[34]
Fe_3O_4/poly($C_3N_3S_3$)	344.8 mg·g^{-1}	25	[35]
rGO–PDTC/Fe_3O_4	181.82 mg·g^{-1}	25	[36]
rGO–poly($C_3N_3S_3$)/Fe_3O_4	400 mg·g^{-1}	25	[37]
CNTs–SH@Fe_3O_4	172.4 mg·g^{-1}	25	[38]
Ggh–g-PAcM/Fe_3O_4	213.8 mg·g^{-1}	30	[39]
Fe_2O_3@SiO_2@SH	98%		[40]
Pec–g-PHEAA/Fe_3O_4	240.2 mg·g^{-1}		[41]

can make $CoFe_2O_4$ particles disperse better and remain stable in water. However, to enhance the ability of $CoFe_2O_4$ to adsorb Hg(II), surface chemical modifications through grafting need to be carried out. Additionally, further embellishments are required to improve the overall performance of $CoFe_2O_4$ in capturing Hg(II) ions [45]. The interaction between cobalt spinel ferrites and mercury (Hg) adsorption is influenced by both surface interactions and magnetic properties, i.e., Hg(II) adsorption onto cobalt spinel ferrites involves chemical bonding, surface interactions, and potential ion exchange, all influenced by the properties of the ferrite and the solution.

Research in this area continues to explore the optimization of cobalt spinal ferrites for effective and efficient Hg(II) removal from various aqueous systems, particularly in the context of water purification and environmental remediation. Therefore, many researchers used a grafting modification to enhance the Hg(II) adsorption efficiency. For example, Zhang et al. synthesized $CoFe_2O_4$–rGO for Hg(II) removal in wastewater and their sorption efficiency was 157.9 $mg \cdot g^{-1}$ [46]. Wang et al. prepared $CoFe_2O_4$@ SiO_2 and achieved an adsorption efficiency of 149.3 $mg \cdot g^{-1}$ on Hg (II) [47] and Xia et al. synthesized $CoFe_2O_4$@ SiO_2–EDTA using a hydrothermal method. The results revealed that the composite material achieved a maximum adsorption efficiency of 103.3 $mg \cdot g^{-1}$ for removing Hg(II) ions [48]. Other cobalt spinal ferrite composites involved in Hg(II) removal includes $CoFe_2O_4$@SiO_2-SH [49], $CoFe_2O_4$@SiO_2@m-SiO_2-SH/NH_2 [50], SH-mSiO_2@$CoFe_2O_4$ [21], $CoFe_2O_4$@SiO_2-Ppy [45], and Py-$CoFe_2O_4$@SiO_2@KCC-1 [44].

This study utilized nanoporous carbon (NC) derived from discarded palm kernel shells to coat a nanocomposite of $CoFe_2O_4$. This coated material has the potential for removing mercury (Hg(II)), aiming to address the environmental risks associated with both heavy metal pollution and agricultural waste. Since the NC is a carbon-rich material with a solid, disordered structure, it can be altered to have high porosity and contains various oxygen-related functional groups like carboxylic acids, phenols, carbonyls, and lactones. These characteristics make it suitable for different applications involving adsorbents. While $CoFe_2O_4$ nanocomposite likely contributes to the composite's magnetic properties, facilitating separation from the treated water. This nanocomposite could serve as an efficient and environmentally friendly solution for addressing mercury pollution in water systems [51,52]. The synthesized NC@$CoFe_2O_4$ nanocomposite was characterized for its surface area (nitrogen adsorption–desorption isotherm), structure (crystalline or amorphous), morphology, thermal stability, magnetization, and functional group(s) prior to be applied for the elimination of Hg(II) ions from a water-based solution. Finally, adsorptive parameters, real application, and adsorption mechanisms were also added to the studies.

2 Materials and methods

2.1 Materials, chemicals, and reagents

Palm kernel shell (NC), iron nitrate ($Fe(NO_3)_2 \cdot 9H_2O$, 99%), cobalt nitrate ($Co(NO_3)_2 \cdot 6H_2O$, 99%), polyethylene glycol 400 (99%), sodium dodecyl sulfate (99%), and ammonia solution were purchased from R&M Chemicals (25%). All chemicals were utilized in their original state without additional purification. Deionized water was employed exclusively for the preparation of solutions in this study.

2.2 Synthesis of NC@$CoFe_2O_4$ nanocomposite

The hydrothermal synthesis procedure for the NC@$CoFe_2O_4$ nanocomposite (Figure 1) consisted of dissolving 6.1 g of Fe $(NO_3)_2 \cdot 9H_2O$ and 4.2 g of $Co(NO_3)_2 \cdot 6H_2O$ in 20 mL of deionized water. Afterward, 5 mL of ammonia solution was added to the mixture. The mixture was stirred for 30 min. Later, various surfactants were added and stirred for an hour again at 35°C to avoid particle precipitation, and pH was adjusted to 10–12. The NC (2 g) was added shortly afterward and the mixture was treated ultrasonically for 2 h and later stirred for 12 h. The end product was moved into an autoclave and heated to 180°C for a duration of 24 h. Afterward, it was spun in a centrifuge and rinsed with both water and ethanol. Finally, the product was dried under vacuum conditions at 70°C overnight to achieve the nanocomposite synthesis.

2.3 Batch adsorption experiments

The effectiveness of the prepared adsorbents in removing metals was assessed using batch adsorption experiments. In a standard experiment, a measured amount of the substance that can capture other substances (adsorbent) was placed into a set of 250 mL flasks. These flasks contained a solution with 100 $mg \cdot L^{-1}$ Hg(II) ions. The flasks were shaken vigorously at room temperature for a duration of 2 h. At specific time intervals, the samples were collected from the flasks, and the concentration of Hg(II) ions in these samples was measured using a MA-3Solo Mercury Analyzer, a specialized instrument.

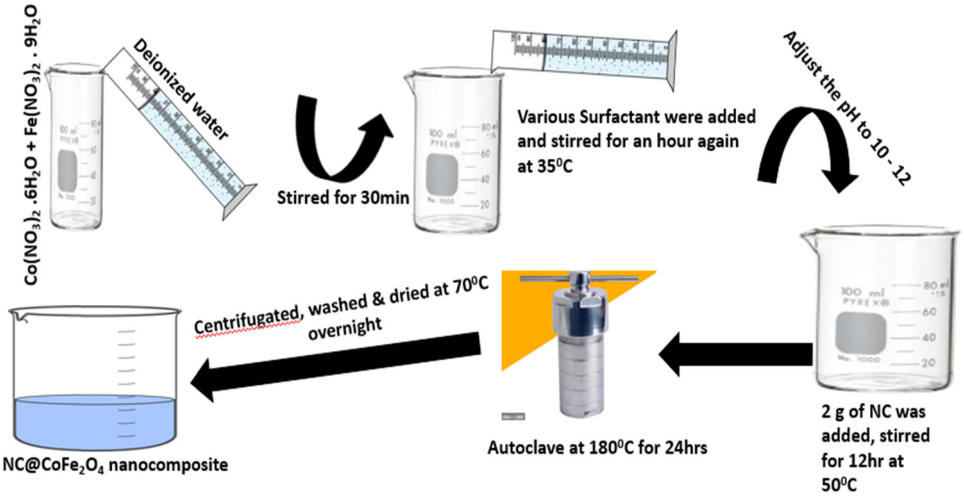

Figure 1: Schematic of the synthesis of the NC@$CoFe_2O_4$ nanocomposite starting from $Co(NO_3)_2$ and $Fe(NO_3)_2$, followed by the addition of surfactant, NC, as well as autoclave, centrifugation, washing, and drying at 70°C.

3 Results and discussion

3.1 Characterization

Table 2 shows a comparison of the textural properties, such as nitrogen adsorption–desorption isotherms, surface area, pore size, and pore volume, between the NC and NC@$CoFe_2O_4$ nanocomposite.

From the comparison of Brunauer-Emmett-Teller (BET)-specific surface area values provided in Table 2, the NC@$CoFe_2O_4$ has an increased value as against the pure NC and is linked to the introduction of $CoFe_2O_4$ NPs onto the NC. At the same time, the NC@$CoFe_2O_4$ nanocomposite has slightly lesser average pore volume and pore sizes as compared to pure NC and thereby providing a hint that the addition of cobalt ferrite NPs are not entirely closing the pores of NC. Similar observations of decreased pore sizes and volumes are also reported in magnetically supported materials, where the main point to consider is the persistence of porosity even after the composite formation [53–55]. Figure 2 illustrates the nitrogen adsorption behavior of the NC@$CoFe_2O_4$ nanocomposite, depending on various types of sorption isotherms. The NC treated with cobalt ferrite NPs showed an isothermal change from Type IV isothermal to Type I isothermal, leading to a decrease in the adsorption of N_2 at high pressure. However, in this case, the Type I isotherm finding indicates microporosity isotherm [56]. Conversely, absorbent materials with larger surface areas are more effective in cleaning pollutants from water and wastewater [57].

As shown in Figure 3a, the NC@$CoFe_2O_4$ nanocomposite exhibits six distinct peaks. These peaks can be attributed to the well-developed crystalline structure of cubic cobalt ferrite. Additionally, a faint peak at 2θ = 25.2–26.6 (002) was observed, indicating the presence of NC in the composite material [46,47,58]. The diffraction peaks of composite material were observed at specific angles, represented as 2θ values, of 30.4°, 35.6°, 43.3°, 53.6°, 57.1°, and 63.1°. These angles correspond to the crystallographic planes of (220), (311), (400), (422), (511), and (440), respectively. This crystal structure is thus assumed to be more favorable for adsorption performance and demonstrated that the major phase was the spinel ferrite composite [2,59]. The reported X-ray diffraction (XRD) patterns are in line with those previously reported for the activated carbon/$CoFe_2O_4$, $CoFe_2O_4$-NP/activated carbon, and thiol-functionalized cobalt ferrite magnetic mesoporous silica (SH-mSiO_2@$CoFe_2O_4$) [21,55,60].

Table 2: Textural properties of NC and NC@$CoFe_2O_4$ nanocomposite materials

Sample	BET surface area ($m^2 \cdot g^{-1}$)	Average pore volume ($cm^3 \cdot g^{-1}$)	Average pore size (nm)
NC	1,280	0.677	2.116
NC@$CoFe_2O_4$	328.9	0.157	1.905

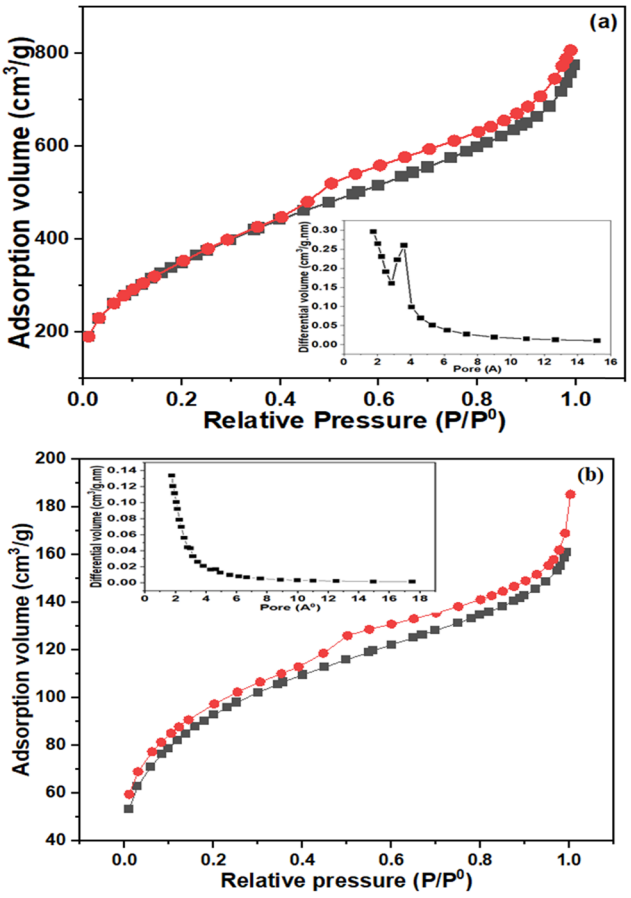

Figure 2: Isotherms of N_2 adsorption–desorption and pore size distribution of the NC (a) and NC@$CoFe_2O_4$ nanocomposite (b).

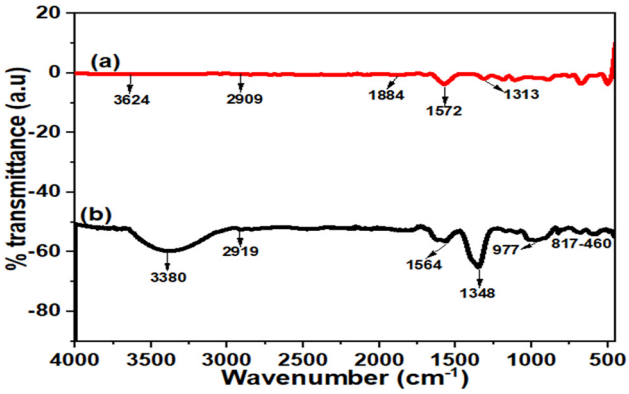

Figure 4: FTIR spectrum of the pure NC (a) and NC@$CoFe_2O_4$ nanocomposite (b).

To understand the magnetic properties of the newly synthesized NC@$CoFe_2O$ nanocomposite, a vibrating sample magnetometer (VSM) was used to measure its magnetic behavior at room temperature. As shown in Figure 3b, the magnetic nature of the NC@$CoFe_2O_4$ nanocomposite exhibited a clear hysteresis appearance, indicating the superparamagnetic behavior [17] with saturation magnetization, retentivity, and coercivity values to be 33.65 emu·g^{-1}, 10.354 Oe, and 418.43 Oe, respectively, which are within the range of those reported for bare $CoFe_2O_4$ particles in previous studies [61–65]. However, the magnetic separation capability of the NC@$CoFe_2O_4$ nanocomposite was confirmed by employing a magnet close to the composite and observing how fast the

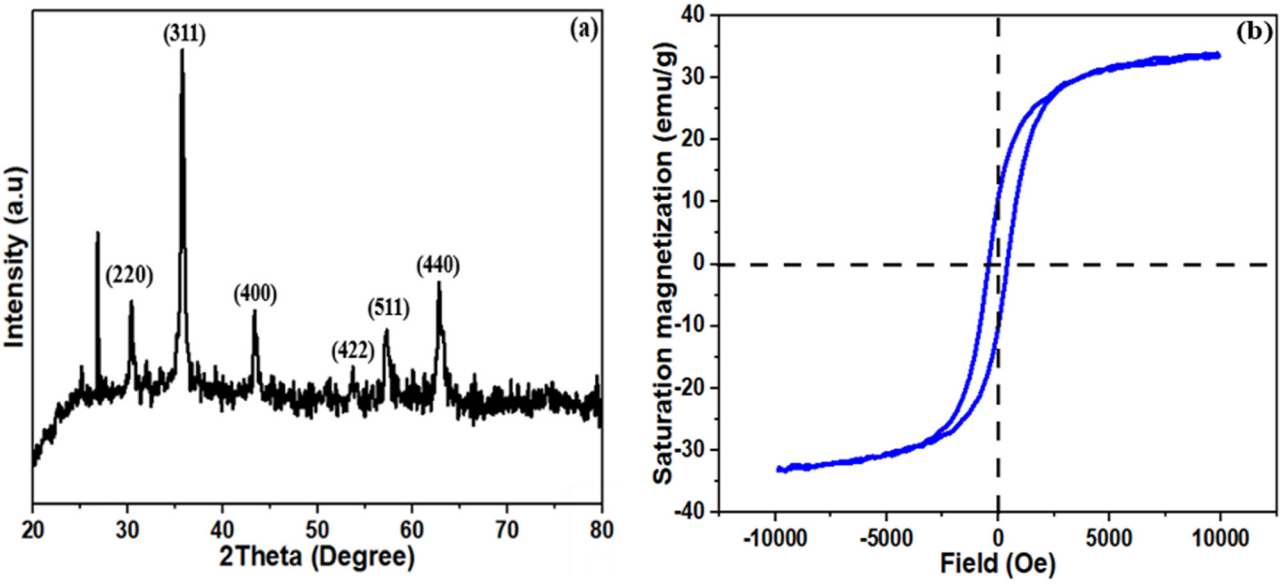

Figure 3: XRD spectrum (a) and magnetization curve (VSM) (b) of the NC@$CoFe_2O_4$ nanocomposite.

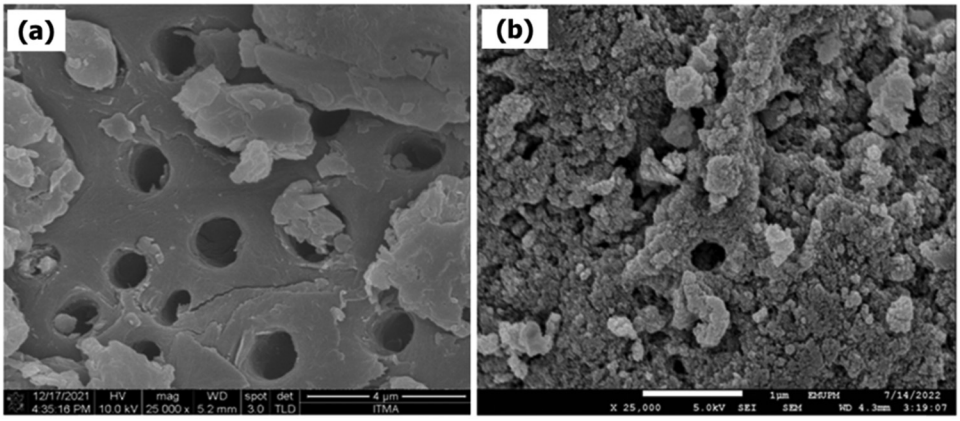

Figure 5: FESEM image of the NC@$CoFe_2O_4$ nanocomposite (a) and NC (b).

black material is drawn near the magnet [38]. This result confirms that the composite can potentially be applied as an adsorbent for the abstraction of heavy metals.

Figure 4b displays the FT-IR spectrum of the NC@$CoFe_2O_4$ nanocomposite. In this spectrum, a significant peak is observed at approximately 3,380 cm^{-1}. This peak is attributed to the stretching vibration of the –OH bond, indicating the presence of physically adsorbed water molecules on the adsorbent material [57,66]. The peak observed at 2,919 cm^{-1} is attributed to the stretching vibration of the –CH group found in the methyl group [64,67]. As mentioned earlier, palm kernel shells were treated with phosphoric acid (H_3PO_4). The presence of phosphorus groups in the NC@$CoFe_2O_4$ nanocomposite is responsible for the observed bands in the range of 970–1,174 cm^{-1} [68,69]. However, the peaks at 1,781, 1,564, and 1,348 cm^{-1} correspond to –C═O, aromatic –C═C, and carboxy –C–O groups on the exterior of the NC@$CoFe_2O_4$ nanocomposite [70,71]. The peak at 817–460 cm^{-1}, shown in Figure 4b, indicates the common distinctive absorption pattern associated with the vibrations of Co–O and Fe–O bands [47,50,72,73], and additionally, the presence of magnetite NPs on the surface of the NC has been confirmed. The appearance of these absorption bands serves as strong evidence that the $CoFe_2O_4$ has effectively combined with the NC, indicating a successful conjugation.

The structure of the NC@$CoFe_2O_4$ nanocomposite appears to generate spots for adsorption, thereby improving the elimination of mercury ions (Hg(II)) from a solution. Morphological characterization of NC (Figure 5a) showed appreciable development of porous structures and higher surface area showing the effect of phosphoric acid evaporation during the carbonization process [67,74]. As shown in Figure 5b, the $CoFe_2O_4$ NPs deposited on the surface of NC are accumulated due to their inherent magnetic interactions

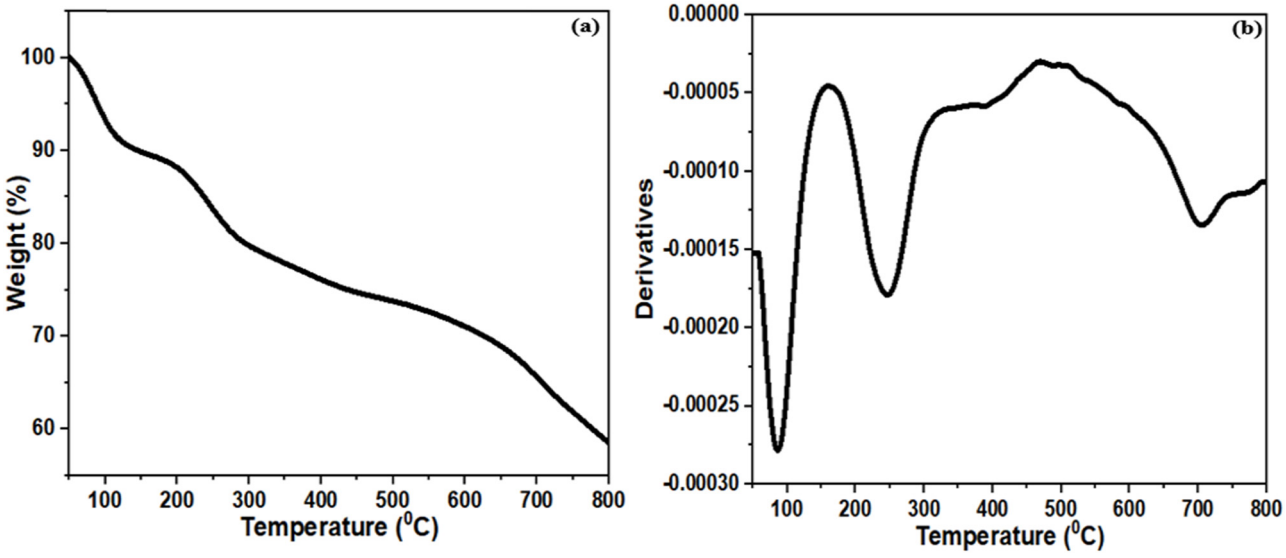

Figure 6: TGA thermogram (a) and DTG profile (b) of thr NC@$CoFe_2O_4$ nanocomposite.

and uniformly showed a regular smooth surface with cracks and cavities, indicating a larger BET value [2,57,72,75].

The thermal stability and degradation pattern were studied by the TGA/DTG analysis. Figure 6a shows the qualitative assessment of the NC@$CoFe_2O_4$ nanocomposite and the graph clearly indicates that the synthesized composite material underwent three significant stages of decomposition. With an initial decomposition temperature below 100°C, the NC@$CoFe_2O_4$ nanocomposite exhibited 9.62% weight loss attributed to the saturated water evaporation. The second weight loss, which occurred at temperatures ranging from 220°C to 260°C, is caused by the breaking of chemically bonded NPs. This is similar to what Choi et al. found when they observed the weight loss occurring between 200°C and 350°C [76]. The final decomposition temperature of the NC@$CoFe_2O_4$ nanocomposite was around 720°C, indicating the stability of this composite at this high temperature (can withstand extreme working conditions). Similar observations were also reported in the $CoFe_2O_4$–graphene oxide composite due to the effective bonding and stability provided by the graphene molecules to the cobalt ferrites [2].

The DTG thermogram of the NC@$CoFe_2O_4$ nanocomposite in Figure 6b showed three degradation steps, with the main step starting below 100°C, followed by a second degradation at 247°C. Finally, the maximum degradation rate due to lignin decomposition at slightly above 700°C confirming the effective coating of the NC material.

3.2 Hg(II) ion adsorption

The effect of various factors like the pH level of the solution, the amount of adsorbent used, the time of contact, the initial concentration of the ion solution, and the temperature of the reaction affect the process of removing Hg(II) from a water-based solution.

3.2.1 Effect of pH

The effectiveness of the NC@$CoFe_2O_4$ nanocomposite in removing Hg(II) was assessed by measuring how well it adsorbed Hg(II) across a range of pH values from 2 to 6. In Figure 7, it is evident that the ability of the NC@$CoFe_2O_4$ nanocomposite to capture Hg(II) ions from a solution increases significantly between pH values 2 and 3. The highest adsorption efficiency for Hg(II) ions, which is 93.2 $mg{\cdot}g^{-1}$, occurs at pH 3. This increase in efficiency can be attributed to the electrostatic interaction that occurs when more negatively charged active sites become available [77]. The pH_{PZC} of NC and NC@$CoFe_2O_4$ is a crucial property that defines the pH at which

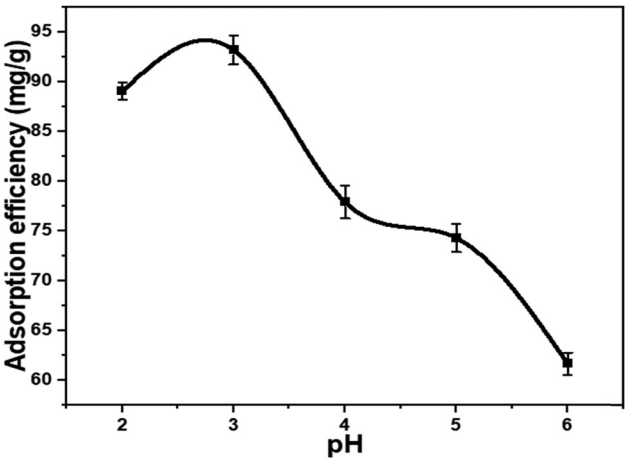

Figure 7: Effect of pH on Hg(II) ion adsorption efficiency of the NC@$CoFe_2O_4$ nanocomposite.

the surface becomes electrically neutral. The pH drift method was used to determine this parameter in this study where the adsorbent materials can remove the ionic species at the desired pH. The pH_{PZC} values for the NC and NC@$CoFe_2O_4$ composite are 3.67 and 4.5, respectively. The measured pH_{PZC} values decrease slightly within a range that results in a negative surface charge. This is attributed to the presence of oxygen-functional groups, which promote the adsorption of cations. Additionally, Tomar and Jeevanandam [62] found that when cations and hydrogen ions both try to stick to the adsorbent surface, they do not compete with each other effectively. This can result in the formation of compounds like $Hg(OH)^+$ and $Hg(OH)_2$. As a consequence, the ability of the NC@$CoFe_2O_4$ nanocomposite to capture pollutants decreases, and it only captures 61.64 $mg{\cdot}g^{-1}$ of Hg(II) ions as pH increases above 3 [78]. A similar pH effect was reported in S-functionalized magnetic metal–organic frameworks and CNT-SH@Fe_3O_4 materials, respectively [38,79]. As a result, pH 3 was selected as the optimum pH for the NC@$CoFe_2O_4$ nanocomposite adsorption experiment in this study.

3.2.2 Effect of dosage adsorbent

The dosage of the NC@$CoFe_2O_4$ nanocomposite was varied between 0.1 and 0.5 g in 100 mL of 10 $mg{\cdot}L^{-1}$ at the optimal pH level of 3 and temperature of 25°C. According to Xia and co-researchers, the concentration of Hg(II) ions in the solution is related to the number of active sites on the surface and the availability of functional groups for the adsorption process. This relationship is illustrated in Figure 8 of the NC@$CoFe_2O_4$ nanocomposite. The results show that the increased amount of adsorbent dosage is expected to increase the percentage of removal. This is a result of the

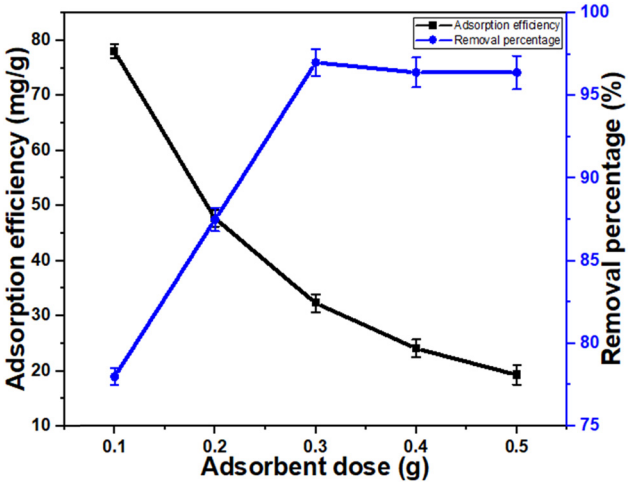

Figure 8: Effect of adsorbent dose on Hg(II) ion adsorption efficiency and the removal percentage of the NC@$CoFe_2O_4$ nanocomposite.

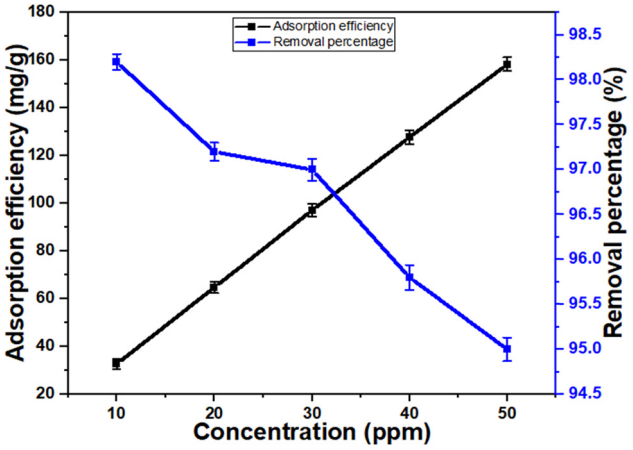

Figure 9: Effect of initial concentration on Hg(II) ion adsorption efficiency and the removal percentage of the NC@$CoFe_2O_4$ nanocomposite.

reaction between COOH and Hg(II) ions [48]. However, the adsorption efficiency of the NC@$CoFe_2O_4$ nanocomposite rapidly decreased as the adsorbent dosage increased. The adsorption efficiency decreased from 78.01 to 19.3 mg·g^{-1} for the NC@$CoFe_2O_4$ nanocomposite and this is because enhancing the adsorbent dosage completely covers the vacant space of the active sites and its saturation in the adsorption process [57]. Several observations have been recorded in various studies that reiterated that the adsorption efficiency decreases with that of the increased adsorbent dosage [49,63,80]. To find the appropriate amount of a substance that can capture other substances from a solution most effectively, how much of this capturing substance should be used was determined. Eventually, the optimal adsorbent dose for the remaining adsorption experiments was resolved to be 0.3 g for the composite.

3.2.3 Effect of Hg(II) ion concentration

The effect of changing the initial concentration of Hg(II) ions in a 100 mL solution, ranging from 10 to 50 mg·L^{-1}, affects the efficiency of adsorption and the percentage of Hg(II) removal on an NC@$CoFe_2O_4$ nanocomposite. As shown in Figure 9, the conditions were as follows: the adsorbent weighed 0.3 g, the duration was 120 min, the temperature was 25°C, and the pH was 3. Lima stated that the primary factor for overcoming the resistance to mass transfer caused by the molecules between the adsorbent material and the adsorbate is the initial concentration of the adsorbent [81]. From the results, it is evident that when the starting concentration of Hg(II) in the solutions increased from 10 to 50 mg·L^{-1}, the ability of the composites to capture Hg(II) increased from 32.7 to 158.3 mg·g^{-1}. As the concentration of the Hg(II) solution increased, the composites made better use of their binding sites, which increased their capacity to adsorb Hg(II) ions [2,82,83]. However, when the starting concentration of Hg(II) solution increased from 10 to 50 mg·L^{-1}, the percentage of Hg(II) removed by the NC@$CoFe_2O_4$ nanocomposite dropped slightly from 98.2% to 95%. This decrease might be because at a higher concentration, the Hg(II) ions either fill the available surface of the nanocomposite or reach a point of saturation. As a result, the removal percentage decreased when the concentration was higher [57,78].

3.2.4 Effect of contact time

Figure 10 shows how the amount of Hg(II) adsorbed by the NC@$CoFe_2O_4$ nanocomposite is related to the time of

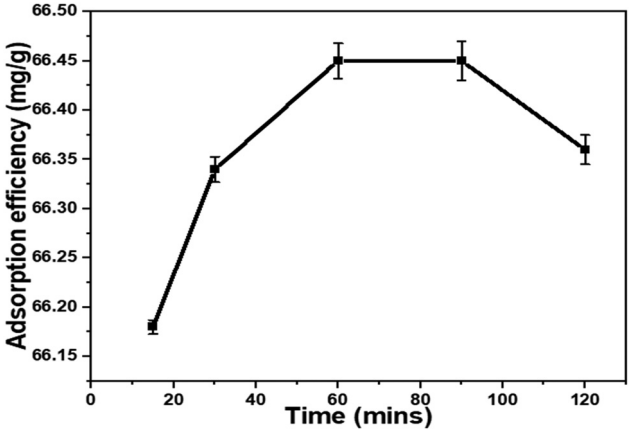

Figure 10: Effect of contact time on Hg(II) ion adsorption efficiency and the removal percentage of the NC@$CoFe_2O_4$ nanocomposite.

contact. The findings indicated that quick adsorption occurs within the initial 60 min, with no significant variation in the adsorption efficiency over the entire contact time [35,64]. The NC@$CoFe_2O_4$ nanocomposite has functional groups that offer numerous active sites. These sites facilitate the quick interaction and bonding of Hg(II) ions within the initial hour of contact [48,78,84]. Despite this, the highest achieved adsorption efficiency is 66.45 mg·g^{-1}, and the ideal contact time is determined to be 60 min.

3.3 Adsorption isotherm studies

In a 100 mL solution, the amount of mercury ions was changed from 10 to 50 mg·L^{-1}, while keeping other factors constant, such as pH at 3 and 0.3 g of the adsorbent. To understand how mercury ions interacted with the adsorbent, the Langmuir and Freundlich isotherms were used to describe this interaction. In simpler terms, the models explained how the concentration of mercury ions in the solution and their attachment to the adsorbent relate to each other using these two models [85].

An adsorption isotherm is crucial for understanding how metal ions and absorbents interact. It helps to determine how molecules are distributed between a solid and liquid when adsorption reaches a balance, revealing the highest efficiency of adsorption. The effectiveness of the NC@$CoFe_2O_4$ nanocomposite in capturing Hg(II) was evaluated by analyzing the data with two different models: the Langmuir and Freundlich isotherms [86]. The Langmuir theory suggests that adsorption occurs at particular uniform spots within the material where it occurs, leading to a single layer of adsorption [79,87]. By contrast, the Freundlich model is typically more suitable for describing processes where adsorption occurs in multiple layers on a surface with uneven characteristics [88]. Eq. 1 shows the Langmuir model in a linear form, while Eq. 2 represents the Freundlich model in a linear form [42,89]:

$$\frac{C_e}{Q_e} = \frac{1}{Q_{max}K_L} + \frac{C_e}{Q_{max}} \quad (1)$$

The equilibrium concentration of Hg(II) ions in a substance, denoted as Q_e (mg·g^{-1}), depends on the affinity of Hg(II) ions for the binding sites on certain composites, represented by K_L, and the equilibrium concentration of Hg(II) ions in the surrounding liquid, denoted as C_e (mg·L^{-1}). The Langmuir isotherm was confirmed in Figure 11, which displayed the relationship between C_e/Q_e and C_e. By analyzing the graph's straight-line equation, the values of Q_{max} and K_L were determined using the slope and intercept:

$$\log Q_e = \log K_F + \frac{1}{n}\log C_e \quad (2)$$

where K_F is the effectiveness of the sorbent in adsorbing Hg(II) ions, and $1/n$ is the concentration of these ions affecting the sorption process. To find these values, a mathematical model called the Freundlich kinetic model was used by plotting the logarithm of the amount of Hg(II) ions adsorbed ($\log Q_e$) against the logarithm of their concentration ($\log C_e$).

The assessment relied on the highest R^2 value obtained from the initial concentration-effect data displayed in a regression plot. In this study, the R^2 values obtained through linear regression for the Langmuir and Freundlich models were 0.9895 and 0.9962, as illustrated in Figure 11 and are presented in Table 3, respectively. The adsorption behavior of Hg(II) adhered more closely to the Freundlich model than the Langmuir model, as indicated by the fact that the correlation coefficient (R^2) for the Freundlich model was higher than that for the Langmuir model. The NC@$CoFe_2O_4$ nanocomposite captures Hg(II) by evenly distributing active adsorption sites across its surface. These sites then attract and adhere to Hg(II) ions on the material's surface [38,78,90]. Meanwhile, the determined R_F value decreases within the range of 0–1.0 (0.0258), which is derived from the K_F values obtained through the Freundlich model. This suggests that the process of Hg(II) adsorption onto the adsorbent was favorable in the study. The highest Hg(II) sorption capacity of the NC@$CoFe_2O_4$ nanocomposite fitted by the Freundlich isothermal model was 232.56 mg·g^{-1}.

3.4 Adsorption kinetic studies

The time for which Hg(II) ion solution adsorption occurs ranges from 15 to 120 min. This experiment was carried out at a pH of 3 and a temperature of 25°C, with an initial concentration of Hg(II) ions set at 30 mg·L^{-1}. To analyze the adsorption process, two kinetic models were employed: the pseudo-first-order rate equation (Eq. 3) and the pseudo-second-order kinetic model (Eq. 4):

$$\ln(q_e - q_t) = \ln q_e - k_t \quad (3)$$

where q_e is the amount of Hg(II) adsorbed onto the surface when equilibrium is reached (mg·g^{-1}), q_t is the amount of Hg(II) adsorbed onto the surface at a specific time t, and k is a constant that describes the speed of the adsorption process and is determined by plotting a graph of the natural logarithm of $\ln(q_e - q_t)$ against t (min^{-1}):

$$\frac{t}{q_t} = \frac{1}{k_2 q_e^2} + \frac{t}{q_e} \quad (4)$$

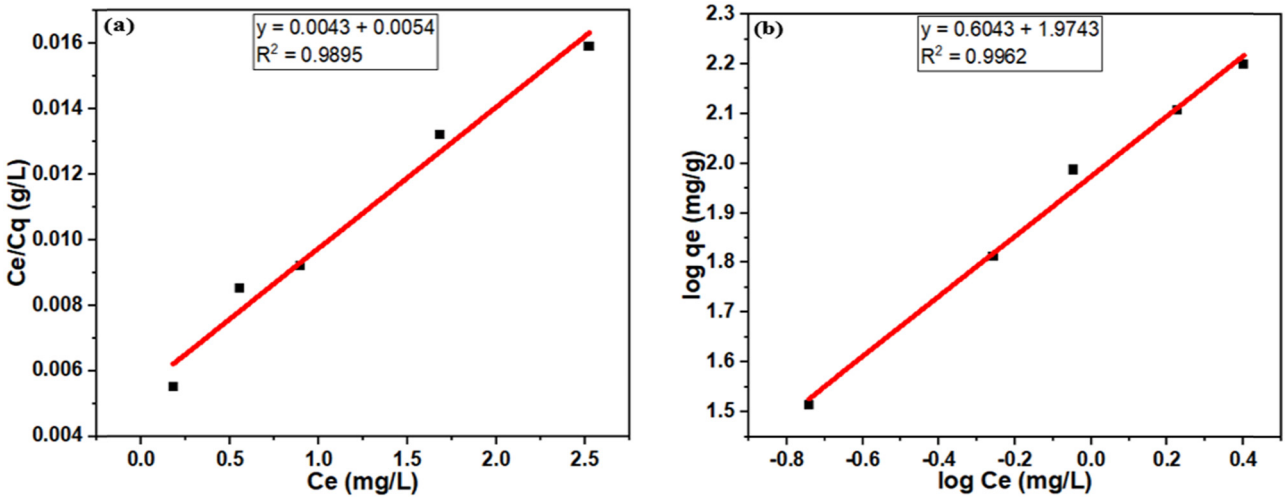

Figure 11: Langmuir (a) and Freundlich (b) model isotherms for Hg(II) adsorption on the NC@$CoFe_2O_4$ nanocomposite.

where t is the time in minutes during which Hg(II) ions are adsorbed, q_t is the quantity of the metal ions adsorbed at a specific time (mg·g^{-1}), and q_e is the amount of metal ions adsorbed at equilibrium (mg·g^{-1}). Additionally, k_2 represents the rate constant for the second-order adsorption process (g·mg^{-1}·min^{-1}).

The following models, pseudo-first and pseudo-second order (Figure 12), are employed to delve deeper into understanding how Hg(II) ions are absorbed by the NC@$CoFe_2O_4$ nanocomposite by studying the time taken to reach equilibrium. The correlation coefficient (R^2) values for the kinetic model fitting were found to be 0.9063 and 0.9999, respectively. These values suggest that the adsorption of Hg(II) ions on the absorbent adhered closely to the pseudo-second-order kinetic model. The experimental result for q_e being fairly similar to the calculated value provides additional evidence that chemisorption played a significant role in this experiment [45,91,92]. Although the pseudo-first-order model may show a strong correlation coefficient (R^2), it is clear that there is a substantial disparity between the actual experimental q_e and the calculated q_e. Consequently, it is evident that the adsorption process does not adhere to the pseudo-first-order model. Table 4 displays the parameters for both the pseudo-first- and pseudo-second-order kinetics models used to describe the sorption of Hg(II) on the NC@$CoFe_2O_4$ nanocomposite.

3.5 Adsorption thermodynamic studies

Thermodynamic investigations were conducted by placing Erlenmeyer flasks in a water bath with temperatures ranging from 25°C to 50°C. This experiment was conducted at pH 3, and the mixture was agitated for 2 h, starting with an initial concentration of 30 mg·L^{-1} Hg(II) ions. The universal gas constant, denoted as R, was utilized to compute essential thermodynamic parameters, including enthalpy (ΔH), entropy (ΔS), and Gibbs free energy (ΔG). The results of these investigations were determined using Eqs. 5 and 6 [93]:

$$\Delta G = -\mathrm{RT}\ln K_\mathrm{d} \tag{5}$$

$$\ln K_\mathrm{d} = -\frac{\Delta H}{\mathrm{RT}} + \frac{\Delta S}{R} \tag{6}$$

where K_d represents a constant that describes how well substances stick to each other when they come into contact, R is a number used in science to help with calculations, and T is the temperature (K). To find the values for ΔH and ΔS, a

Table 3: Langmuir and Freundlich isotherm model parameters for Hg(II) adsorption by the NC@$CoFe_2O_4$ nanocomposite

Langmuir isotherm			Fruendlich isotherm		
Maximum adsorption capacity (mg·g^{-1})	**Langmuir constant, K_L (L·mg^{-1})**	**Correlation coefficient, R^2**	**Freundlich constant, K_F (mg·g^{-1})**	**Freundlich constant, n**	**Correlation coefficient, R^2**
232.56	1.256	0.9895	5.366	1.65	0.9962

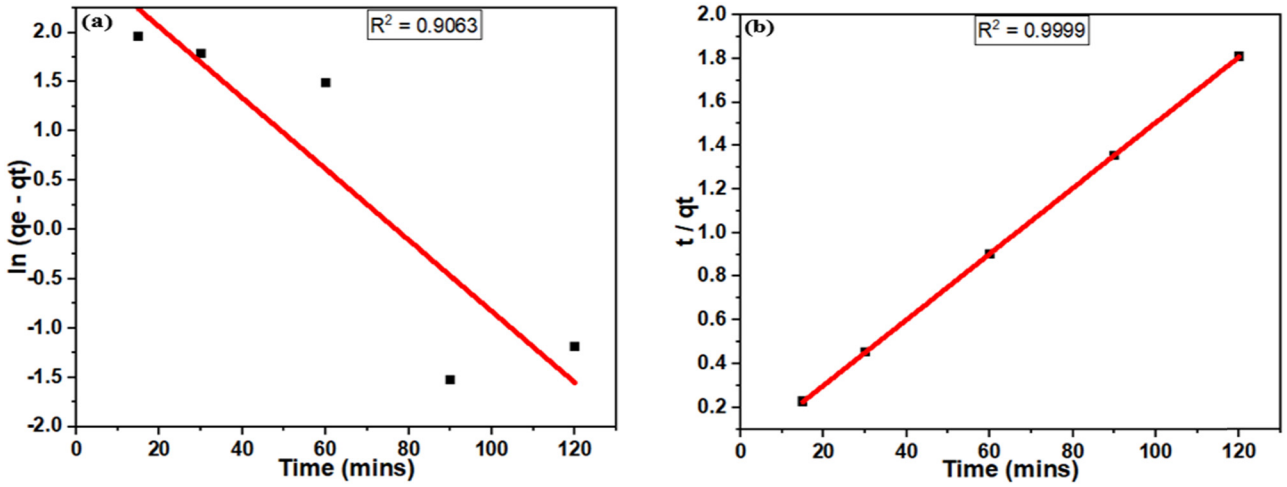

Figure 12: Pseudo-first-order model (a) and pseudo-second-order model (b) for Hg(II) adsorption on the NC@$CoFe_2O_4$ nanocomposite.

graph of the logarithm of K_d vs the reciprocal of temperature (1/T) was plotted These values help in understanding the heat and entropy changes that occur during this adsorption process.

Adsorption is significantly affected by the environment's temperature. Thermodynamic properties can also help in determining if adsorption is likely to occur and whether the process is spontaneous or not. The changes in sorption effectiveness as temperature increases also reveal whether a process is endothermic or exothermic [49,94]. Figure 13a shows the effect of temperature change on adsorption and removal percentage of Hg(II) onto the NC@$CoFe_2O_4$ nanocomposite. According to the graph, as the temperature increases from 25°C to 50°C, both the effectiveness of adsorption and the percentage of material removed show a slight improvement. This suggests that the adsorption process becomes more effective and favorable at higher temperatures, indicating it is an endothermic reaction. As the temperature increases, the energy associated with the movement of Hg(II) molecules also increases. This is explained by the kinetic theory, which suggests that these molecules interact with the surface they are adsorbed on through collisions [72,95].

Figure 13b shows the Van't Hoff plot utilized to estimate the changes in free energy (ΔG), enthalpy (ΔH), and entropy (ΔS) associated with the process of Hg(II) adsorption on the NC@$CoFe_2O_4$ nanocomposite. Moreover, the computed energy change values listed in Table 5 demonstrate negative values of ΔG with increased temperature, indicating that the adsorption mechanism of the absorbent is a spontaneous process as a result of constant mobility increment and diffusion of ions into its pores [93]. The positive enthalpy, ΔH, and entropy, ΔS, values implied that the NC@$CoFe_2O_4$ nanocomposite adsorption toward Hg(II) is an endothermic reaction and that the probability of favorable adsorption mechanism randomly increases, displaying a strong affinity between Hg(II) and the adsorbate [42,48,55,61].

The influence of the pH studies of NC@$CoFe_2O_4$ (Figure 7) supports the formation of negatively charged surfaces, which favors the cationic adsorption studies and, in our case, the Hg(II) ions. Likewise, the adsorbent and adsorbate dosage studies of NC@$CoFe_2O_4$ (Figures 8 and 9) have indicated that the Hg(II) adsorption at the porous sites occurs only through physicochemical and van der Waals attractions. A rapid increase in the adsorbent dosage is expected to have supported the complete coverage of the adsorbent material's active vacant spaces and so saturation in the adsorption procedure was achieved. Additionally, the isotherm adsorption studies (Figure 11) and kinetic models (Figure 12 indicate the Hg(II) recovery onto the NC@$CoFe_2O_4$ composite to be more suited by the Fruendlich model with pseudo-second order, meaning the process occurs on the multi-layer heterogeneous surface and is chemisorbed. Finally, adsorption thermodynamics (Figure 13) are observed with a positive enthalpy and entropy, i.e., Hg(II) adsorption on NC@$CoFe_2O_4$ is endothermic with strong affinity among the

Table 4: Parameters of the pseudo-first- and pseudo-second-order kinetic models for Hg(II) adsorption by the NC@$CoFe_2O_4$ nanocomposite

Kinetic models	q_e, experimental (mg·g^{-1})	q_e, calculated (mg·g^{-1})	Correlation coefficient R^2
Pseudo-first order	66.45	7.55	0.9063
Pseudo-second order	66.45	66.23	0.9999

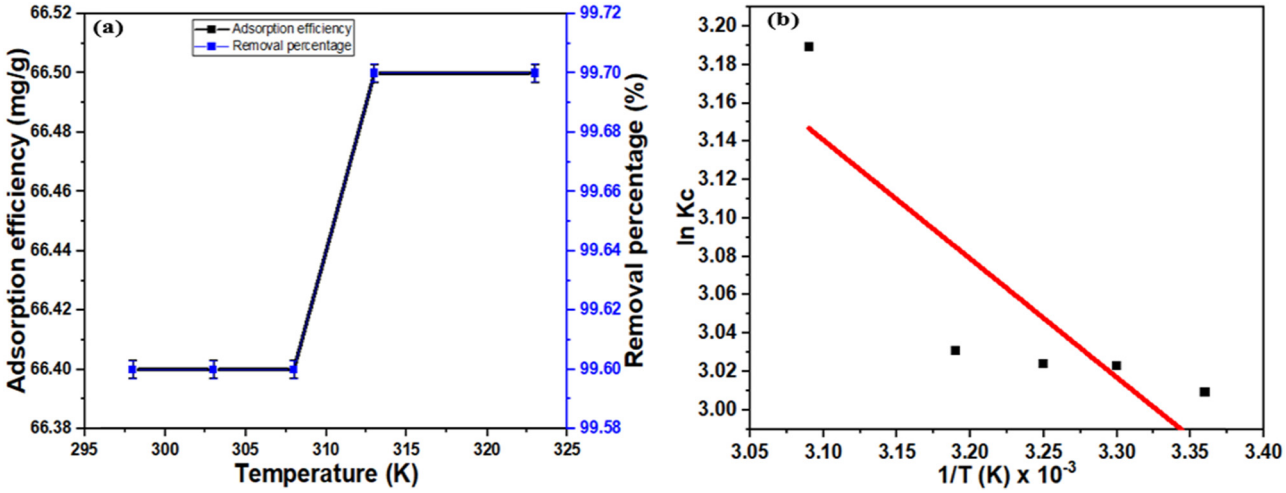

Figure 13: Effect of temperature for Hg(II) adsorption (a) and Van't Hoff plot used to calculate the activation energy for Hg(II) adsorption (b) on the NC@$CoFe_2O_4$ nanocomposite.

Hg(II) ions and the functional groups attached to NC and $CoFe_2O_4$. Overall, the nanocomposite with its porous architecture offered by the carbonaceous base originating from the natural palm kernel shell in conjugation with the solid magnetic support ($CoFe_2O_4$) allows for the natural recovery of positively charged Hg(II) ions in aqueous solutions. The porous nanocomposite adsorbent base with its negative charge on its surface of active sites allows for the spontaneous and natural adsorption (no requirement of additional energies like stirring, heating, light, etc.) of Hg(II) ions. Such natural localization provides more stabilization to the adsorbent Hg(II) ions through physicochemical and electrostatic attractions at the multi-layer heterogeneous surfaces, thereby confirming the effective performance of our NC@$CoFe_2O_4$ nanocomposite.

3.6 Testing of NC@$CoFe_2O_4$ nanocomposite toward real wastewater sample

To test the efficacy of our developed NC@$CoFe_2O_4$ nanocomposite in practical applications, the adsorbent was employed to remove Hg(II) ions under the previously mentioned optimized conditions. In that view, the real wastewater samples of condensate having a mercury concentration of 0.214 mg·L^{-1} collected from the petroleum (oil and natural gas) industry were tested against our NC@$CoFe_2O_4$ adsorbate using a mercury analyzer. The results of adsorption studies confirmed the removal of 93% Hg(II) ions, corresponding to 0.199 mg·L^{-1} of the condensate of the petroleum industry. This confirms the effective adsorption behavior of the NC@$CoFe_2O_4$ nanocomposite towards Hg(II) removal available in industrial wastewaters and at the same time highlights its attractive features like low costs, larger and easy production, natural origin, and magnetic nature.

4 Conclusion

The NC@$CoFe_2O_4$ nanocomposite was successfully synthesized using a hydrothermal technique. The prepared composite exhibited a saturation magnetization capability of 33.650 emu·g^{-1}, with maximum adsorption efficiency of 232.56 mg·g^{-1} toward Hg(II) at pH 3. The adsorption

Table 5: Studies of thermodynamic parameters for Hg(II) adsorption by the NC@$CoFe_2O_4$ nanocomposite

Temperature (K)	Δ*S* (kJ·mol^{-1}·K^{-1})	Δ*H* (kJ·mol^{-1})	Δ*G* (kJ·mol^{-1})
298	42.05	5.14	−7.46
303			−7.62
308			−7.74
313			−7.89
323			−8.56

isotherm was effectively combined with the Freundlich isotherm model, and the kinetic analysis was conducted using the pseudo-second-order reaction. Moreover, the adsorption mechanism aligns well with spontaneous and endothermic reactions, as evidenced by the negative free energy and positive enthalpy/entropy values. Additionally, the NC@$CoFe_2O_4$ nanocomposite material, which was successfully synthesized, demonstrated effectiveness in detecting and removing Hg(II) from actual waste condensate in the oil and gas industry. The NC@$CoFe_2O_4$ nanocomposite demonstrates notable contributions to Hg(II) removal in a green environment through its high adsorption capacity, magnetic retrievability, regenerability, selective removal, low energy consumption, and compatibility with green technologies. These features collectively make it a promising and environmentally friendly material for mercury remediation applications.

Funding information: This work was supported by the Ministry of Higher Education (MOHE), Malaysia, under the Prototype Research Grant Scheme (PRGS) and Universiti Putra Malaysia. Also, the KSU authors acknowledge the funding from Researchers Supporting Project number (RSP2023R54), King Saud University, Riyadh, Saudi Arabia.

Author contributions: Lawal Abubakar: conceptualization, methodology, investigation, writing original draft, and review and editing; Nor Azah Yusof: methodology, validation, formal analysis, and supervision; Abdul Halim Abdullah: formal analysis, data curation, and supervision; Mohd Hanif Wahid: validation, formal analysis, and resources; Siti Fatimah Abd Rahman: validation, data curation, and resources; Faruq Mohammad: writing original draft, and review and editing; Hamad A. Al-Lohedan: supervision and funding acquisition; and Ahmed A. Soleiman: formal analysis and project administration. All authors agreed to publish this version of the manuscript.

Conflict of interest: The authors state no conflict of interest.

Data availability statement: Data sharing is not applicable to this article as no datasets were generated or analysed during the current study.

References

[1] Sustainable Development Goals. https://www.un.org/sustainabledevelopment/sustainable-development-goals/ (accessed April 2020).

[2] Ren H, Li H, Fan H, Qi G, Liu Y. Facile synthesis of $CoFe_2O_4$-graphene oxide nanocomposite by high-gravity reactor for removal of Pb(II). Sep Purif Technol. 2023;305:122472. doi: 10.1016/j.seppur.2022.122472.

[3] Chakraborty R, Asthana A, Singh AK, Jain B, Susan ABH. Adsorption of heavy metal ions by various low-cost adsorbents: a review. Int J Environ Anal Chem. 2022;102(2):342–79. doi: 10.1080/03067319.2020.1722811.

[4] Awual MR, Urata S, Jyo A, Tamada M, Katakai A. Arsenate removal from water by a weak-base anion exchange fibrous adsorbent. Water Res. 2008;42(3):689–96. doi: 10.1016/j.watres.2007.08.020.

[5] Arora R. Adsorption of heavy metals–a review. Mater Today: Proc. 2019;18:4745–50. doi: 10.1016/j.matpr.2019.07.462.

[6] Ma J, Qin G, Zhang Y, Sun J, Wang S, Jiang L. Heavy metal removal from aqueous solutions by calcium silicate powder from waste coal fly-ash. J Clean Prod. 2018;182:776–82. doi: 10.1016/j.jclepro.2018.02.115.

[7] Arrifano GDP, Augusto-Oliveira M, Lopes-Araújo A, Santos-Sacramento L, Macchi BM, Nascimento JLMD, et al. Global Human Threat: The Potential Synergism between Mercury Intoxication and COVID-19. Int J Environ Res Public Health. 2023;20(5):4207. doi: 10.3390/ijerph20054207.

[8] Saha S, Dhara K, Chukwuka AV, Pal P, Saha NC, Faggio C. Sub-lethal acute effects of environmental concentrations of inorganic mercury on hematological and biochemical parameters in walking catfish, Clarias batrachus. Comp Biochem Physiol Part C: Toxicol Pharmacol. 2023;264:109511. doi: 10.1016/j.cbpc.2022.109511.

[9] Johs A, Eller VA, Mehlhorn TL, Brooks SC, Harper DP, Mayes MA, et al. Dissolved organic matter reduces the effectiveness of sorbents for mercury removal. Sci Total Environ. 2019;690:410–6. doi: 10.1016/j.scitotenv.2019.07.001.

[10] Beckers F, Awad YM, Beiyuan J, Abrigata J, Mothes S, Tsang DC, et al. Impact of biochar on mobilization, methylation, and ethylation of mercury under dynamic redox conditions in a contaminated floodplain soil. Environ Int. 2019;127:276–90. doi: 10.1016/j.envint.2019.03.040.

[11] Shan Y, Yang W, Li Y, Liu Y, Pan J. Preparation of microwave-activated magnetic bio-char adsorbent and study on removal of elemental mercury from flue gas. Sci Total Environ. 2019;697:134049. doi: 10.1016/j.scitotenv.2019.134049.

[12] Abbas K, Znad H, Awual MR. A ligand anchored conjugate adsorbent for effective mercury (II) detection and removal from aqueous media. Chem Eng J. 2018;334:432–43. doi: 10.1016/j.cej.2017.10.054.

[13] Nodehi R, Shayesteh H, Rahbar-Kelishami A. Fe_3O_4@ NiO core–shell magnetic nanoparticle for highly efficient removal of Alizarin red S anionic dye. Int J Environ Sci Technol. 2022;19(4):2899–912. doi: 10.1007/s13762-021-03399-8.

[14] Nodehi R, Shayesteh H, Kelishami AR. Enhanced adsorption of congo red using cationic surfactant functionalized zeolite particles. Microchem J. 2020;153:104281. doi: 10.1016/j.microc.2019.104281.

[15] Shayesteh H, Raji F, Kelishami AR. Influence of the alkyl chain length of surfactant on adsorption process: a case study. Surf Interfaces. 2021;22:100806. doi: 10.1016/j.surfin.2020.100806.

[16] Gopal RA, Song M, Yang D, Lkhagvaa T, Chandrasekaran S, Choi D. Synthesis of hierarchically structured ɤ-Fe_2O_3–PPy nanocomposite as effective adsorbent for cationic dye removal from wastewater. Environ Pollut. 2020;267:115498. doi: 10.1016/j.envpol.2020.115498.

[17] Zare Pirhaji J, Moeinpour F, Mirhoseini Dehabadi A, Yasini Ardakani SA. Experimental study and modelling of effective parameters on removal of Cd(II) from water by halloysite/graphene quantum dots magnetic nanocomposite as an adsorbent using

response surface methodology. Appl Organomet Chem. 2020;34(7):e5640. doi: 10.1002/aoc.5640.
[18] Moeinpour F, Kamyab S, Akhgar MR. $NiFe_2O_4$ magnetic nanoparticles as an adsorbent for cadmium removal from aqueous solution. J Water Chem Technol. 2017;39:281–8. doi: 10.3103/S1063455X17050058.
[19] Yu S, Wang X, Pang H, Zhang R, Song W, Fu D, et al. Boron nitride-based materials for the removal of pollutants from aqueous solutions: a review. Chem Eng J. 2018;333:343–60. doi: 10.1016/j.cej.2017.09.163.
[20] Baby R, Hussein MZ, Abdullah AH, Zainal Z. Nanomaterials for the treatment of heavy metal contaminated water. Polymers. 2022;14(3):583. doi: 10.3390/polym14030583.
[21] Li K, Xie L, Hao Z, Xiao M. Effective removal of Hg (II) ion from aqueous solutions by thiol functionalized cobalt ferrite magnetic mesoporous silica composite. J Dispers Sci Technol. 2020;41(4):503–9. doi: 10.1080/01932691.2019.1591974.
[22] Kazemi M, Ghobadi M, Mirzaie A. Cobalt ferrite nanoparticles ($CoFe_2O_4$ MNPs) as catalyst and support: magnetically recoverable nanocatalysts in organic synthesis. Nanotechnol Rev. 2018;7(1):43–68. doi: 10.1515/ntrev-2017-0138.
[23] Liosis C, Papadopoulou A, Karvelas E, Karakasidis TE, Sarris IE. Heavy metal adsorption using magnetic nanoparticles for water purification: A critical review. Materials. 2021;14(24):7500. doi: 10.3390/ma14247500.
[24] Mahmoud ME, Ahmed SB, Osman MM, Abdel-Fattah TM. A novel composite of nanomagnetite-immobilized-baker's yeast on the surface of activated carbon for magnetic solid phase extraction of Hg(II). Fuel. 2015;139:614–21. doi: 10.1016/j.fuel.2014.09.002.
[25] Song J, Kong H, Jang J. Adsorption of heavy metal ions from aqueous solution by polyrhodanine-encapsulated magnetic nanoparticles. J Colloid Interface Sci. 2011;359(2):505–11. doi: 10.1016/j.jcis.2011.04.034.
[26] Sun L, Li Y, Sun M, Wang H, Xu S, Zhang C, et al. Porphyrin-functionalized Fe_3O_4@ SiO_2 core/shell magnetic colorimetric material for detection, adsorption and removal of Hg^{2+} in aqueous solution. N J Chem. 2011;35(11):2697–704. doi: 10.1039/C1NJ20307J.
[27] Zhang C, Sui J, Li J, Tang Y, Cai W. Efficient removal of heavy metal ions by thiol-functionalized superparamagnetic carbon nanotubes. Chem Eng J. 2012;210:45–52. doi: 10.1016/j.cej.2012.08.062.
[28] Mahapatra A, Mishra BG, Hota G. Electrospun Fe_2O_3–Al_2O_3 nanocomposite fibers as efficient adsorbent for removal of heavy metal ions from aqueous solution. J Hazard Mater. 2013;258:116–23. doi: 10.1016/j.jhazmat.2013.04.045.
[29] Guo X, Du B, Wei Q, Yang J, Hu L, Yan L, et al. Synthesis of amino functionalized magnetic graphenes composite material and its application to remove Cr (VI), Pb (II), Hg (II), Cd (II) and Ni (II) from contaminated water. J Hazard Mater. 2014;278:211–20. doi: 10.1016/j.jhazmat.2014.05.075.
[30] Qi X, Li N, Xu Q, Chen D, Li H, Lu J. Water-soluble Fe_3O_4 superparamagnetic nanocomposites for the removal of low concentration mercury (II) ions from water. RSC Adv. 2014;4(88):47643–8. doi: 10.1039/C4RA05935B.
[31] Chen Z, Geng Z, Zhang Z, Ren L, Tao T, Yang R, et al. Synthesis of magnetic Fe_3O_4@ C nanoparticles modified with–SO_3H and–COOH groups for fast removal of Pb^{2+}, Hg^{2+}, and Cd^{2+} ions. Eur J Inorg Chem. 2014;2014(20):3172–7. doi: 10.1002/ejic.201301500.
[32] Cui L, Wang Y, Gao L, Hu L, Yan L, Wei Q, et al. EDTA functionalized magnetic graphene oxide for removal of Pb (II), Hg (II) and Cu (II) in water treatment: adsorption mechanism and separation property. Chem Eng J. 2015;281:1–10. doi: 10.1016/j.cej.2015.06.043.
[33] Wang Z, Xu J, Hu Y, Zhao H, Zhou J, Liu Y, et al. Functional nanomaterials: Study on aqueous Hg (II) adsorption by magnetic Fe_3O_4@ SiO_2-SH nanoparticles. J Taiwan Inst Chem Eng. 2016;60:394–402. doi: 10.1016/j.jtice.2015.10.041.
[34] Mahmoud ME, Amira MF, Zaghloul AA, Ibrahim GA. High performance microwave-enforced solid phase extraction of heavy metals from aqueous solutions using magnetic iron oxide nanoparticles-protected-nanosilica. Sep Purif Technol. 2016;163:169–72. doi: 10.1016/j.seppur.2016.02.039.
[35] Fu W, Huang Z. One-pot synthesis of a two-dimensional porous Fe_3O_4/Poly ($C_3N_3S_3$) network nanocomposite for the selective removal of Pb (II) and Hg (II) from synthetic wastewater. ACS Sustain Chem Eng. 2018;6(11):14785–94. doi: 10.1021/acssuschemeng.8b03320.
[36] Fu W, Huang Z. Magnetic dithiocarbamate functionalized reduced graphene oxide for the removal of Cu (II), Cd (II), Pb (II), and Hg (II) ions from aqueous solution: Synthesis, adsorption, and regeneration. Chemosphere. 2018;209:449–56. doi: 10.1016/j.chemosphere.2018.06.087.
[37] Fu W, Wang X, Huang Z. Remarkable reusability of magnetic Fe_3O_4-encapsulated $C_3N_3S_3$ polymer/reduced graphene oxide composite: a highly effective adsorbent for Pb and Hg ions. Sci Total Environ. 2019;659:895–904. doi: 10.1016/j.scitotenv.2018.12.303.
[38] Fan L, Zhou A, Zhong L, Zhang Z, Liu Y. Selective and effective adsorption of Hg (II) from aqueous solution over wide pH range by thiol functionalized magnetic carbon nanotubes. Chemosphere. 2019;226:405–12. doi: 10.1016/j.chemosphere.2019.03.154.
[39] Kulal P, Badalamoole V. Efficient removal of dyes and heavy metal ions from waste water using Gum ghatti–graft–poly (4-acryloylmorpholine) hydrogel incorporated with magnetite nanoparticles. J Environ Chem Eng. 2020;8(5):104207. doi: 10.1016/j.jece.2020.104207.
[40] Subana PS, Manjunatha C, Rao BM, Venkateswarlu B, Nagaraju G, Suresh R. Surface functionalized magnetic α-Fe_2O_3 nanoparticles: synthesis, characterization and Hg^{2+} ion removal in water. Surf Interfaces. 2020;21:100680. doi: 10.1016/j.surfin.2020.100680.
[41] Kulal P, Badalamoole V. Magnetite nanoparticle embedded Pectin-graft-poly (N-hydroxyethylacrylamide) hydrogel: Evaluation as adsorbent for dyes and heavy metal ions from waste water. Int J Biol Macromol. 2020;156:1408–17. doi: 10.1016/j.ijbiomac.2019.11.181.
[42] Rafie SF, Abdollahi H, Sayahi H, Ardejani FD, Aghapoor K, Darvanjooghi MHK, et al. Genetic algorithm-assisted artificial neural network modelling for remediation and recovery of Pb (II) and Cr(VI) by manganese and cobalt spinel ferrite super nanoadsorbent. Chemosphere. 2023;321:138162. doi: 10.1016/j.chemosphere.2023.138162.
[43] Foroutan R, Mohammadi R, MousaKhanloo F, Sahebi S, Ramavandi B, Kumar PS, et al. Performance of montmorillonite/graphene oxide/$CoFe_2O_4$ as a magnetic and recyclable nanocomposite for cleaning methyl violet dye-laden wastewater. Adv Powder Technol. 2020;31(9):3993–4004. doi: 10.1016/j.apt.2020.08.001.
[44] Radhakrishnan K, Panneerselvam P, Ravikumar A, Morad N. Magnetic core-shell fibrous silica functionalized with pyrene derivative for highly sensitive and selective detection of Hg(II) ion. J Dispers Sci Technol. 2019;40(9):1368–77. doi: 10.1080/01932691.2018.1468265.

[45] Zhao Y, Xia K, Zhang Z, Zhu Z, Guo Y, Qu Z. Facile synthesis of polypyrrole-functionalized $CoFe_2O_4$@ SiO_2 for removal for Hg(II). Nanomaterials. 2019;9(3):455. doi: 10.3390/nano9030455.
[46] Zhang Y, Yan L, Xu W, Guo X, Cui L, Gao L, et al. Adsorption of Pb(II) and Hg(II) from aqueous solution using magnetic $CoFe_2O_4$-reduced graphene oxide. J Mol Liq. 2014;191:177–82. doi: 10.1016/j.molliq.2013.12.015.
[47] Wang X, Zhang Z, Zhao Y, Xia K, Guo Y, Qu Z, et al. A mild and facile synthesis of amino functionalized $CoFe_2O_4$@ SiO_2 for Hg (II) removal. Nanomaterials. 2018;8(9):673. doi: 10.3390/nano8090673.
[48] Xia K, Guo Y, Shao Q, Zan Q, Bai R. Removal of mercury (II) by EDTA-functionalized magnetic $CoFe_2O_4$@ SiO_2 nanomaterial with core-shell structure. Nanomaterials. 2019;9(11):1532. doi: 10.3390/nano9111532.
[49] Zhu H, Shen Y, Wang Q, Chen K, Wang X, Zhang G, et al. Highly promoted removal of Hg (II) with magnetic $CoFe_2O_4$@ SiO_2 core–shell nanoparticles modified by thiol groups. RSC Adv. 2017;7(62):39204–15. doi: 10.1039/C7RA06163C.
[50] Zhang Z, Xia K, Pan Z, Yang C, Wang X, Zhang G, et al. Removal of mercury by magnetic nanomaterial with bifunctional groups and core-shell structure: Synthesis, characterization and optimization of adsorption parameters. Appl Surf Sci. 2020;500:143970. doi: 10.1016/j.apsusc.2019.143970.
[51] Heidarinejad Z, Dehghani MH, Heidari M, Javedan G, Ali I, Sillanpää M. Methods for preparation and activation of activated carbon: a review. Environ Chem Lett. 2020;18:393–415. doi: 10.1007/s10311-019-00955-0.
[52] Benedetti V, Patuzzi F, Baratieri M. Characterization of char from biomass gasification and its similarities with activated carbon in adsorption applications. Appl Energy. 2018;227:92–9. doi: 10.1016/j.apenergy.2017.08.076.
[53] Yang N, Zhu S, Zhang D, Xu S. Synthesis and properties of magnetic Fe_3O_4-activated carbon nanocomposite particles for dye removal. Mater Lett. 2008;62(4–5):645–7. doi: 10.1016/j.matlet.2007.06.049.
[54] Castro CS, Guerreiro MC, Gonçalves M, Oliveira LC, Anastácio AS. Activated carbon/iron oxide composites for the removal of atrazine from aqueous medium. J Hazard Mater. 2009;164(2–3):609–14. doi: 10.1016/j.jhazmat.2008.08.066.
[55] Ai L, Huang H, Chen Z, Wei X, Jiang J. Activated carbon/$CoFe_2O_4$ composites: facile synthesis, magnetic performance and their potential application for the removal of malachite green from water. Chem Eng J. 2011;156(2):243–9. doi: 10.1016/j.cej.2009.08.028.
[56] Bastami TR, Entezari MH. Activated carbon from carrot dross combined with magnetite nanoparticles for the efficient removal of p-nitrophenol from aqueous solution. Chem Eng J. 2012;210:510–9. doi: 10.1016/j.cej.2012.08.011.
[57] Malakootian M, Nasiri A, Mahdizadeh H. Preparation of $CoFe_2O_4$/activated carbon@ chitosan as a new magnetic nanobiocomposite for adsorption of ciprofloxacin in aqueous solutions. Water Sci Technol. 2018;78(10):2158–70. doi: 10.2166/wst.2018.494.
[58] Song J, Wang Y, Lv Z, Li Y, Cao XQ, Cheng W. Degradation of nonylphenol ethoxylate 10 in biochar-$CoFe_2O_4$/peroxymonosulfate system: Transformation products identification, catalysis mechanism and influencing factors. J Environ Chem Eng. 2023;11(1):109241. doi: 10.1016/j.jece.2022.109241.
[59] Ghanbari D, BandehAli S, Moghadassi A. Embedded three spinel ferrite nanoparticles in PES-based nano filtration membranes with enhanced separation properties. Main Group Met Chem. 2021;45(1):1–10. doi: 10.1515/mgmc-2022-0001.
[60] Mehrabi F, Vafaei A, Ghaedi M, Ghaedi AM, Dil EA, Asfaram A. Ultrasound assisted extraction of Maxilon Red GRL dye from water samples using cobalt ferrite nanoparticles loaded on activated carbon as sorbent: optimization and modeling. Ultrason Sonochem. 2017;38:672–80. doi: 10.1016/j.ultsonch.2016.08.012.
[61] Kaveh R, Bagherzadeh M. Simultaneous removal of mercury ions and cationic and anionic dyes from aqueous solution using epichlorohydrin cross-linked chitosan@ magnetic Fe_3O_4/activated carbon nanocomposite as an adsorbent. Diam Relat Mater. 2022;124:108923. doi: 10.1016/j.diamond.2022.108923.
[62] Tomar D, Jeevanandam P. Synthesis of cobalt ferrite nanoparticles with different morphologies via thermal decomposition approach and studies on their magnetic properties. J Alloy Compd. 2020;843:155815. doi: 10.1016/j.jallcom.2020.155815.
[63] Huang Y, Wang W, Feng Q, Dong F. Preparation of magnetic clinoptilolite/$CoFe_2O_4$ composites for removal of Sr^{2+} from aqueous solutions: kinetic, equilibrium, and thermodynamic studies. J Saudi Chem Soc. 2017;21(1):58–66. doi: 10.1016/j.jscs.2013.09.005.
[64] Ren C, Ding X, Fu H, Meng C, Li W, Yang H. Preparation of amino-functionalized $CoFe_2O_4$@ SiO_2 magnetic nanocomposites for potential application in absorbing heavy metal ions. RSC Adv. 2016;6(76):72479–86. doi: 10.1039/C6RA13304E.
[65] Wu H, Liu G, Wang X, Zhang J, Chen Y, Shi J, et al. Solvothermal synthesis of cobalt ferrite nanoparticles loaded on multiwalled carbon nanotubes for magnetic resonance imaging and drug delivery. Acta Biomater. 2011;7(9):3496–504. doi: 10.1016/j.actbio.2011.05.031.
[66] Xu Z, Li W, Xiong Z, Fang J, Li Y, Wang Q, et al. Removal of anionic dyes from aqueous solution by adsorption onto amino-functionalized magnetic nanoadsorbent. Desalin Water Treat. 2016;57(15):7054–65. doi: 10.1080/19443994.2015.1012748.
[67] Wang Y, Li H, He Z, Guan J, Qian K, Hu J. Removal of elemental mercury from flue gas using cobalt-containing biomaterial carbon prepared from contaminated Iris sibirica biomass. ACS Omega. 2020;5(12):6288–98. doi: 10.1021/acsomega.9b03605.
[68] Liou TH. Development of mesoporous structure and high adsorption capacity of biomass-based activated carbon by phosphoric acid and zinc chloride activation. Chem Eng J. 2010;158(2):129–42. doi: 10.1016/j.cej.2009.12.016.
[69] Parlayıcı Ş, Pehlivan E. Removal of metals by Fe_3O_4 loaded activated carbon prepared from plum stone (Prunus nigra): kinetics and modelling study. Powder Technol. 2017;317:23–30. doi: 10.1016/j.powtec.2017.04.021.
[70] Li X, Feng J, Du Y, Bai J, Fan H, Zhang H, et al. One-pot synthesis of $CoFe_2O_4$/graphene oxide hybrids and their conversion into FeCo/graphene hybrids for lightweight and highly efficient microwave absorber. J Mater Chem A. 2015;3(10):5535–46. doi: 10.1039/C4TA05718J.
[71] Li N, Zheng M, Chang X, Ji G, Lu H, Xue L, et al. Preparation of magnetic $CoFe_2O_4$-functionalized graphene sheets via a facile hydrothermal method and their adsorption properties. J Solid State Chem. 2011;184(4):953–8. doi: 10.1016/j.jssc.2011.01.014.
[72] Asadi R, Abdollahi H, Boroumand Z, Kisomi AS, Darvanjooghi MHK, Magdouli S, et al. Intelligent modelling for the elimination of lanthanides (La^{3+}, Ce^{3+}, Nd^{3+} and Eu^{3+}) from aqueous solution by magnetic $CoFe_2O_4$ and $CoFe_2O_4$-GO spinel ferrite nanocomposites. Environ Pollut. 2022;309:119770. doi: 10.1016/j.envpol.2022.119770.
[73] Yavari S, Mahmodi NM, Teymouri P, Shahmoradi B, Maleki A. Cobalt ferrite nanoparticles: preparation, characterization and

anionic dye removal capability. J Taiwan Inst Chem Eng. 2016;59:320–9. doi: 10.1016/j.jtice.2015.08.011.
[74] Lee J, Kim S, Shin H. Hierarchical porous carbon electrodes with sponge-like edge structures for the sensitive electrochemical detection of heavy metals. Sensors. 2021;21(4):1346. doi: 10.3390/s21041346.
[75] Tabit R, Amadine O, Essamlali Y, Dânoun K, Rhihil A, Zahouily M. Magnetic $CoFe_2O_4$ nanoparticles supported on graphene oxide ($CoFe_2O_4$/GO) with high catalytic activity for peroxymonosulfate activation and degradation of rhodamine B. RSC Adv. 2018;8(3):1351–60. doi: 10.1039/C7RA09949E.
[76] Choi KM, Kil HS, Lee YS, Lim DY, Cho SB, Lee BW. Preparation and luminescence properties of $SrTiO_3$: Pr^{3+}, Al^{3+} phosphor from the glycolate method. J Lumin. 2011;131(5):894–9. doi: 10.1016/j.jlumin.2010.12.020.
[77] Razak MR, Yusof NA, Aris AZ, Nasir HM, Haron MJ, Ibrahim NA, et al. Phosphoric acid modified kenaf fiber (K-PA) as green adsorbent for the removal of copper (II) ions towards industrial waste water effluents. React Funct Polym. 2020;147:104466. doi: 10.1016/j.reactfunctpolym.2019.104466.
[78] Gheitasi F, Ghammamy S, Zendehdel M, Semiromi FB. Removal of mercury (II) from aqueous solution by powdered activated carbon nanoparticles prepared from beer barley husk modified with thiol/Fe_3O_4. J Mol Struct. 2022;1267:133555. doi: 10.1016/j.molstruc.2022.133555.
[79] Xu C, He M, Chen B, Hu B. Modulated synthesis of S-functionalized magnetic metal organic frameworks-808 for Hg (II) removal. J Clean Prod. 2023;387:135859. doi: 10.1016/j.jclepro.2023.135859.
[80] Wang K, Chen K, Xiang L, Zeng M, Liu Y, Liu Y. Relationship between Hg (II) adsorption property and functional group of different thioamide chelating resins. Sep Purif Technol. 2022;292:121044. doi: 10.1016/j.seppur.2022.121044.
[81] Lima EC. Removal of emerging contaminants from the environment by adsorption. Ecotoxicol Environ Saf. 2018;150:1–17. doi: 10.1016/j.ecoenv.2017.12.026.
[82] Liu Z, Sun Y, Xu X, Qu J, Qu B. Adsorption of Hg(II) in an aqueous solution by activated carbon prepared from rice husk using KOH activation. ACS Omega. 2020;5(45):29231–42. doi: 10.1021/acsomega.0c03992.
[83] Li B, Yin W, Xu M, Tan X, Li P, Gu J, et al. Facile modification of activated carbon with highly dispersed nano-sized α-Fe_2O_3 for enhanced removal of hexavalent chromium from aqueous solutions. Chemosphere. 2019;224:220–7. doi: 10.1016/j.chemosphere.2019.02.121.
[84] Repo E, Warchol JK, Kurniawan TA, Sillanpää ME. Adsorption of Co (II) and Ni (II) by EDTA-and/or DTPA-modified chitosan: kinetic and equilibrium modeling. Chem Eng J. 2010;161(1–2):73–82. doi: 10.1016/j.cej.2010.04.030.
[85] Jena KK, Reddy KSK, Karanikolos GN, Choi DS. L-Cysteine and silver nitrate based metal sulfide and Zeolite-Y nano adsorbent for efficient removal of mercury (II) ion from wastewater. Appl Surf Sci. 2023;611:155777. doi: 10.1016/j.apsusc.2022.155777.
[86] Ebelegi AN, Ayawei N, Wankasi D. Interpretation of adsorption thermodynamics and kinetics. Open J Phys Chem. 2020;10(03):166. http://www.scirp.org/journal/Paperabs.aspx?PaperID=102369.
[87] Wang J, Guo X. Adsorption kinetic models: Physical meanings, applications, and solving methods. J Hazard Mater. 2020;390:122156. doi: 10.1016/j.jhazmat.2020.122156.
[88] Ragadhita R, Nandiyanto ABD. How to calculate adsorption isotherms of particles using two-parameter monolayer adsorption models and equations. Indonesian J Sci Technol. 2021;6(1):205–34. doi: 10.17509/ijost.v6i1.32354.
[89] Aliyu M, Abdullah AH, bin Mohamed Tahir MI. Adsorption tetracycline from aqueous solution using a novel polymeric adsorbent derived from the rubber waste. J Taiwan Inst Chem Eng. 2022;136:104333. doi: 10.1016/j.jtice.2022.104333.
[90] Hakami O, Zhang Y, Banks CJ. Thiol-functionalised mesoporous silica-coated magnetite nanoparticles for high efficiency removal and recovery of Hg from water. Water Res. 2012;46(12):3913–22. doi: 10.1016/j.watres.2012.04.032.
[91] Zhang S, Qian L, Zhou Y, Guo Y. High selective removal towards Hg (II) from aqueous solution with magnetic diatomite-based adsorbent functionalized by poly (3-aminothiophenol): conditional optimization, application, and mechanism. Environ Sci Pollut Res. 2023;30:1–16. doi: 10.1007/s11356-023-26070-w.
[92] Fito J, Nkambule TT. Synthesis of biochar-$CoFe_2O_4$ nanocomposite for adsorption of methylparaben from wastewater under full factorial experimental design. Environ Monit Assess. 2023;195(1):241. doi: 10.1007/s10661-022-10819-w.
[93] Al-Salehin PZ, Moeinpour F, Mohseni-Shahri FS. Adsorption isotherm and thermodynamic studies of As (III) removal from aqueous solutions using used cigarette filter ash. Appl Water Sci. 2019;9(8):1–8. doi: 10.1007/s13201-019-1059-9.
[94] Raghav S, Kumar D. Adsorption equilibrium, kinetics, and thermodynamic studies of fluoride adsorbed by tetrametallic oxide adsorbent. J Chem Eng Data. 2018;63(5):1682–97. doi: 10.1021/acs.jced.8b00024.
[95] Rasheed T, Shafi S, Bilal M, Hussain T, Sher F, Rizwan K. Surfactants-based remediation as an effective approach for removal of environmental pollutants-A review. J Mol Liq. 2020;318:113960. doi: 10.1016/j.molliq.2020.113960.